https://doi.org/10.5194/amt-2021-163
Preprint. Discussion started: 11 August 2021

Atmospheric Measurement Techniques Discussions

New sampling strategy removes imaging spectroscopy solar-smearing bias in sub-km vapour scaling statistics

Mark T. Richardson[1,2], David R. Thompson[1], Marcin J. Kurowski[1], Matthew D. Lebsock[1]

[1]Jet Propulsion Laboratory, California Institute of Technology, Pasadena, CA 91109, USA
[2]Department of Atmospheric Science, Colorado State University, Fort Collins, CO 90095, USA

Correspondence to: Mark Richardson (markr@jpl.nasa.gov)

Abstract. Upcoming spaceborne imaging spectrometers will allow retrieval of total column water vapour (TCWV) over land at horizontal resolution of 30—80 m. Here we show how to obtain, from these retrievals, exponents describing the power-law scaling of sub-km horizontal variability in clear-sky bulk planetary boundary layer (PBL) water vapour (q). Using large-eddy simulations (LES) of shallow convective PBLs we show how sunlight entering the PBL up to several km away from the footprint location degrades estimates of these exponents. We address this by calculating exponents perpendicular to the solar azimuth, that is to say flying "across" the sunlight path rather than "towards" or "away" from the Sun. Across 23 LES snapshots, at SZA=60° the mean bias in calculated exponent is 38±12 % (95 % range) along the solar azimuth, while following our strategy it is 3±9 % and no longer significant. Both bias and root-mean-square error RMSE decrease with lower SZA. We include retrieval errors from several sources including: (1) the Earth Surface Mineral Dust Source Investigation (EMIT) instrument noise model, (2) requisite assumptions about the atmospheric thermodynamic profile, and (3) spatially nonuniform aerosol distributions. This technique can be used to obtain unique information about sub-km PBL q scaling from upcoming spaceborne spectrometer missions, while mitigating errors due to challenging solar geometries.

1 Introduction

Spatial scaling in the variability of atmospheric properties such as water vapour (q) can be characterised via structure functions, with the n^{th} order structure function of a field $f(x)$, S_n defined as:

$$S_n(r) = E[(f(x) - f(x+r))^n] \quad (1)$$

Where $E[]$ is the expected value, x a location and r a separation between points. Fields of temperature (T), q and wind-speed are commonly well-modelled by a power law:

$$S_n(r) \propto r^{\zeta_n} \quad (2)$$

https://doi.org/10.5194/amt-2021-163
Preprint. Discussion started: 11 August 2021

Atmospheric Measurement Techniques Discussions

Such that ζ_n is the log-log gradient of S_n as a function of r. There is strong motivation to quantify and understand these exponents and the ranges Δr within which they are valid, and here we specify second-order structure functions S_2 with exponent ζ_2, describing variance scaling. This is related to the commonly-referenced Fourier power spectrum exponent β:

$$\beta = -(\zeta_2 + 1) \quad (3)$$

One motivation for obtaining these exponents is that climate model sub-grid variability in q is strongly linked to cloud formation (Golaz et al., 2002; Perraud et al., 2011; Sommeria and Deardorff, 1977). In principle sub-grid variance can be tuned for each model setup, but scale-aware variance relationships allow a smooth and consistent transition between low (order ~hundreds of km) and high (order ~km) resolution models (Arakawa et al., 2011; Schemann et al., 2013).

At scales larger than model grid cells, observational estimates of variance scaling can also be used to assess model performance, as has been done using estimates of temperature (T) and q from Atmospheric Infrared Sounder (AIRS) and airborne campaign data (Kahn et al., 2011).

Furthermore, the scaling exponents are related to the physical processes that generate the cascade of turbulent eddies in the atmosphere. For example, while mean-scale statistics retrieved by AIRS are approximately isotropic in the horizontal, there are differences in scaling between the horizontal and vertical (Pressel and Collins, 2012). Scaling following ζ_2=2/3 is predicted for a passive tracer in the inertial range of three-dimensional locally isotropic turbulence following Kolmogorov theory. Accounting for the buoyancy effects can strongly modify that scaling (Bolgiano, 1959; Obukhov, 1959), with different exponents expected for the velocity (ζ_2=6/5-7/5) and scalars (ζ_2=2/5), as shown in, e.g. Kunnen et al. (2008), Wroblewski et al. (2010) or Boffetta et al. (2012). Exponents of 7/5 have been commonly measured for vertical wind profiles from dropsondes (Lovejoy et al., 2007), and values typically near ζ_2 of 6/5 for horizontal water vapour in non-convective areas, and ζ_2=0.72 in convective areas have been determined from airborne lidar retrievals over horizontal ranges of up to 100 km (Fischer et al., 2012, 2013), meanwhile the sub-km regime remains undermeasured.

Of particular interest for modellers are the existence of "scale breaks", distances at which the exponents change such that a smooth transition between model resolutions may not be possible. These have been calculated to occur at distances over a broad range of 10—1000 km (Bacmeister et al., 1996; Gage and Nastrom, 1985; Kahn et al., 2011; Pinel et al., 2012) and the range of scales has been speculated to be related to the size of convective systems (Dorrestijn et al., 2018) or changes in the nature of turbulence (Kurowski et al., 2015; Skamarock et al., 2014).

This study focusses on the estimation of horizontal scaling of clear-sky TCWV at sub-km scales, and specifically on the integrated PBL water vapour which we refer to as the partial column water vapour ($PCWV_{PBL}$). Recent work using airborne data (Thompson et al., 2021) and large eddy simulation (LES) output (Richardson et al., 2021) has provided evidence that sub-km horizontal variability in total column water vapour (TCWV) is almost perfectly correlated with $PCWV_{PBL}$ variability, such that high-spatial-resolution retrievals of TCWV from visible and shortwave infrared (VSWIR) imaging spectrometers can provide unique information about PBL q variability. This is not a statement that all water vapour is inside the PBL, rather that on sub-km spatial scales, the variability in low-altitude water vapour dominates the horizontal column variability. It remains a

https://doi.org/10.5194/amt-2021-163
Preprint. Discussion started: 11 August 2021


Atmospheric Measurement Techniques Discussions

challenge to disentangle variability from different heights within the PBL such as the sub-cloud layer or a conditionally unstable cloud layer, which may have different scaling properties.

In particular, the PBL depth is typically 1—2.5 km in these simulations, while we obtain variability statistics over horizontal ranges of under 1 km. The vertical averaging over a scale larger than the horizontal calculation means that the interpretation of the physical meaning of the derived exponents is challenging and may not be directly related to the theoretically derived exponents discussed above. This study aims only to determine whether the measurement problem of the solar path can be overcome, and leaves the physical interpretation out of scope. This point will be revisited in Section 4.

Several modern and upcoming missions obtain or will obtain VSWIR spectra that could allow retrieval of TCWV at horizontal resolutions from 20—100 m. Current examples include the Multi-Spectral Imager (MSI) on Sentinel-2 (Drusch et al., 2012), the PRecursore IperSpettrale della Missione Applicativa (PRISMA, Candela et al. (2016)) and DLR Earth Sensing Imaging Spectrometer (DESIS, Krutz et al. (2019)). Upcoming missions such as NASA's Earth Surface Mineral Dust Source Investigation (EMIT; Green and Thompson (2020)) and ESA's Copernicus Hyperspectral Imaging Mission for the Environment (CHIME; e.g. Rast et al. (2019)) will obtain horizontal resolution of order 30—80 m, and this study will assess performance assuming footprint sizes of 40—50 m, i.e. at the mid-point of that range.

This footprint selection was made based on the resolution of available LES output, and the analysis method is based on the output of retrievals developed specifically for EMIT, which primarily retrieves TCWV to allow atmospheric correction for its surface reflectance target observable. Other instruments such as PRISMA or MSI may have different error characteristics, but we treat retrieval errors in a general manner that could be expanded to these other instruments.

This study attempts to determine whether EMIT will be able to obtain ζ_2 over 0.5—1 km after accounting for (1) random retrieval error, (2) systematic biases in retrieval mean and sensitivity and (3) solar zenith angle.

The PBL is of particular interest since it is the location where reflective low clouds form and in Dorrestijn et al. (2018)'s analysis, ζ_2 varied more in the 850 hPa layer than the 300 hPa or 500 hPa layers. However, previous analyses have generally been restricted to far larger spatial ranges with Dorrestijn et al. (2018) referring to 55—165 km scale variance as occurring at the "tiny scale". Other examples at higher resolution generally use airborne measurements, with few calculations for separations under 1 km using onboard sensors (Cho et al., 1999), using lidar at 5—100 km (Fischer et al., 2013) or evaluating simulations with lidar for separations >11 km (Selz et al., 2017).

This study uses LES outputs and does not make any statements about the realism or cause of the LES output ζ_2 values, but instead aims solely to identify and quantify retrieval biases and errors. Its greatest contribution is to demonstrate that directional calculation strategies can remove biases in estimates of ζ_2 introduced by the solar path through the atmosphere. For illustration, consider a PBL of 2 km depth being viewed at nadir with a solar zenith angle (SZA) of 30°, and note that the sunlight enters the PBL >1 km away from the nominal surface target. This effectively coarsens the horizontal resolution, potentially destroying the benefits of a nominal 50 m footprint for atmospheric investigation. For this reason Thompson et al. (2021) only used flight lines with very low SZA to calculate ζ_2. This paper uses the solar-path-traced outputs of Richardson et al. (2021) to demonstrate

https://doi.org/10.5194/amt-2021-163
Preprint. Discussion started: 11 August 2021


Atmospheric Measurement Techniques Discussions

that by calculating the structure function in a direction perpendicular to the solar azimuth, the bias in ζ_2 is removed for calculations within the 23 LES snapshots considered.

If this result can be extended to the real-world, then upcoming high-spatial-resolution spaceborne VSWIR spectrometers will provide a breakthrough for analysis of moisture scaling across unprecedented spatial scales. Our retrievals are restricted to clear sky areas over land, but this still represents a substantial advance on the current capacities of other instrument types. Lidar measurements avoid the solar-path issue, and can retrieve vertical information including above clouds, but current and anticipated spaceborne lidars do not offer VSWIR's fine spatial resolution or broad spatial coverage from a wide swath. Sounders such as infrared can profile the atmosphere, but have footprints that are too large for sub-km exploration.

Even airborne measurements, which offer far less coverage than spaceborne sensors, may suffer from their own challenges. Evidence suggests that the tendency of flights to follow isobars rather than maintain altitude can introduce height variations that blend vertical variation into horizontal calculations and result in exponents similar to those predicted due to buoyancy's vertical effect (Lovejoy et al., 2004; Pinel et al., 2012).

The VSWIR sampling technique introduced here could greatly expand the range of conditions under which spatial scaling of water vapour can be quantified. In Section 2 we describe the LES output, simulated retrievals, and how retrieval errors and solar path are accounted for in calculation of ζ_2. Section 3 presents the results and Section 4 discusses and concludes.

2 Data and Methods

2.1 Large Eddy Simulation output

We use output from the five LES runs of shallow convection as in Richardson et al. (2021), with four cloudy cases (ARM, ARM_lsconv, BOMEX, RICO) and one case in which clouds do not form (DRY). Simulations use two models, EULAG for the ARM cases (Prusa et al., 2008) and JPL-UCONN LES for the others (Matheou and Chung, 2014). Simulation setups are described in Richardson et al. (2021) and the associated references (Brown et al., 2002; Kurowski et al., 2020; Matheou and Chung, 2014; Siebesma et al., 2003; vanZanten et al., 2011), and while some simulations represent oceanic boundary layers we simply assume a land surface for the retrievals. Static reanalysis profiles from MERRA-2 (Gelaro et al., 2017) are appended above the LES domain, but the LES domains were shown to capture horizontal variability in q from analysis of LES output and airborne lidar profiles over the Pacific (Bedka et al., 2021). The 23 selected snapshots are labelled by their timestamp, e.g. DRY_7200s represents two hours into the DRY simulation. The vapour q_v and liquid water q_c fields are extracted from these snapshots and then TCWV is calculated from the appropriate pressure-weighted vertical sum. The LES output horizontal resolution ranges from Δx=20—50 m, here we degrade the Δx=20 m cases to Δx=40 m resolution to make the spatial difference statistics more consistent.

SZA ranges from 0—60° inclusive in increments of 15°, and the solar ray is traced along the selected SZA from the top of atmosphere to the centre of a surface grid cell, and then directly up to represent a nadir viewing instrument. The solar azimuth

https://doi.org/10.5194/amt-2021-163
Preprint. Discussion started: 11 August 2021


Atmospheric Measurement Techniques Discussions

angle is the positive y direction in each simulation, such that the sunlight's horizontal path component is in the negative y direction. Path q_v is pressure weighted to obtain path column water vapour, which we also refer to as TCWV. Footprints are flagged as cloudy or shaded if their cloud water path CWP>1×10^{-3} mm, with CWP calculated in the same manner as the TCWV but using liquid water content, and this threshold represents approximately τ<0.3 in a subadiabatic cloud (Szczodrak et al., 2001). A footprint is masked if it is cloudy or shaded for any SZA, and by using a common mask we isolate the effect of SZA and retrieval errors from changes due to sampling.

2.2 Generating retrieved TCWV fields

Richardson et al. (2021) adopted an emulator approach for full-scene simulation due to computational constraints. We use those emulators here, which obtain retrieved $TCWV_{ret}$ from input TCWV, which is in fact the integrated water path along the solar path, via:

$$TCWV_{ret} = a_1 TCWV + a_2 + \epsilon \quad , \tag{4}$$

Where a_1 and a_2 are the slope and intercept and ε a random sample from a Normal distribution whose standard deviation σ_ε quantifies the random retrieval error. The parameter a_1 represents the sensitivity $dTCWV_{ret}/dTCWV$ and a_2 is related to the bias, although it is only equal to the bias if a_1=1. Some errors in a_1 can be understood as due to erroneous atmospheric profiles assumed in the current retrieval implementation. The parameters were fit to a sample of retrievals that used plane-parallel radiative transfer with profiles directly from the LES columns (i.e. without solar path tracing) and SZA=45°. In sensitivity tests, SZA>45° led to somewhat larger σ_ε but later we show that our structure-function conclusions will not be affected even if different SZAs change the emulator parameters.

The emulators were fit to subsets of retrievals that used the Imaging Spectrometer Optimal Fitting (Isofit) code (Thompson et al., 2018, 2019), with the MODTRAN6.0 radiative transfer model used for both forward and inverse calculations (Berk et al., 2014, 2015). Richardson et al. (2021) showed that Eq. (4) is valid for a scene with varying aerosol optical depth, but that the emulator parameters depend on the surface classification and atmospheric conditions. The primary requirements are that parameters are fit separately to each type of PBL, represented by different LES runs (i.e. for each case, all snapshots within a case use the same parameters), and that an observed region is either a mixture of vegetation or a mixture of mineral surfaces alone. Each LES simulation has one emulator to convert TCWV to $TCWV_{ret}$, and the same emulator is used to obtain $TCWV_{ret}$ from all SZA path TCWVs.

2.3 Calculation of spatial statistics and removal of random error

$S_2(r)$ is calculated from the LES field of $TCWV_{ret}$ in one horizontal direction at a time, by including all pairs of footprints separated by r in that direction provided that neither of the footprints in the pair is flagged as cloudy or shadowed for any SZA. To calculate along the LES x axis, each different y location is effectively treated as a 1-D field and its set of $f(x+r)-f(x)$ values are calculated, then all the 1-D subsets are concatenated and the reported $S_2(r)$ is the expectation value of this combined dataset.

https://doi.org/10.5194/amt-2021-163
Preprint. Discussion started: 11 August 2021


Atmospheric Measurement Techniques Discussions

The horizontal directions are either along the x axis ("perpendicular" to the sunlight) or along the y axis (the "parallel" case). Figure 1 displays example $S_2(r)$ for clear-sky TCWV and their associated scaling parameters, i.e., $dln(S_2)/dln(r)$, showing that ζ_2 will depend on the range of r over which it is calculated. The variation of ζ_2 with Δr can be due to changes in physical processes in addition to imperfect process representation in the LES, such as nonphysical dissipation at separations smaller than several grid cells (Brown et al., 2002). This study is not concerned with the interpretation of ζ_2 but rather with the accuracy with which it can be obtained, so we do not explore this further and follow Thompson et al. (2021) in calculating the fit over r=0.5—1 km.

We estimate and remove the measurement noise following the method of Richardson et al. (2021). They derived a structure-function-based method to estimate σ_ε from the retrieved TCWV field, thereby allowing better estimation of S_2 by subtracting $2\sigma_\epsilon^2$ from Eq. (5). This method involves calculating S_2 in one horizontal direction at r=Δx (i.e. separation of 1 grid cell, 40 m or 50 m), then smoothing the field by a factor of two in the perpendicular direction and recalculating S_2, which we label $S_{2,\times2}$. At these small separations, $2\sigma_\epsilon^2 \gg a_1^2 S_2(r)$, such that $S_{2,\times2} - S_2 \approx 2\sigma_\epsilon^2$.

We evaluate the sensitivity of our derived ζ_2 to uncertainty in the retrieval emulator, when calculating S_2 from the retrieved fields the emulator changes the retrieved value $S_{2,ret}$ as:

$$S_{2,ret}(r) = a_1^2 S_2(r) + 2\sigma_\epsilon^2 \quad (5)$$

And the estimated $\zeta_{2,ret}$ is;

$$\zeta_2 = \frac{d\ln(a_1^2 S_2 + 2\sigma_\epsilon^2)}{d\ln(r)} \quad (6)$$

This shows that both biases in a_1 ("retrieval sensitivity") and the magnitude of random errors can change the derived ζ_2. Richardson et al., (2021) showed that errors in a_1 were the largest source of uncertainty in the estimating the spatial standard deviation. We will therefore perform sensitivity tests for a range of a_1 values, and show only one σ_ε case since results were insensitive to changes in σ_ε up to a factor of four scaling.

The final question we address is whether the scaling exponent estimated at the very high spatial resolution of missions such as EMIT will be fundamentally different from that obtained by current sensors such as MERIS and MODIS that can provide TCWV at a nominal resolution near Δx≈250 m. Large-scale σ_x narrows as spatial resolution coarsens, but it is not clear how this affects the spatial scaling properties considered here, so for this test we sequentially degrade a TCWV field from Δx=50 m to Δx=250 m and calculate S_2 and ζ_2 at each resolution.

3 Results

3.1 Variation of horizontal ζ_2 with height

Figure 2 shows how the ζ_2 calculated for PCWV integrated up to different heights varies within the PBL, but that the value becomes fixed by the PBL top. That is, estimates made from TCWV refer to the value for $PCWV_{PBL}$, but this conceals vertical

https://doi.org/10.5194/amt-2021-163
Preprint. Discussion started: 11 August 2021


Atmospheric Measurement Techniques Discussions

structure within the PBL. We can therefore confirm that our derived values are indeed representative of bulk PBL statistics, but further work is needed to determine the precise utility of statistics of $PCWV_{PBL}$ and furthermore, we note that corresponding estimates of PBL height from other sources may be necessary to help interpret measurements of $PCWV_{PBL}$ scaling.

3.2 Retrieval errors and ζ_2

The results from all sensitivity tests applied to the clear-sky TCWV in the ARM_18000s snapshot are shown in Figure 3, results are similar for other snapshots (not shown). Figure 3(a) shows that random errors that we estimate will be typical for EMIT result in substantial changes to calculated $\ln(S_2)/\ln(r)$, with a notable flattening over much of the r range and an unacceptably large error in ζ_2 derived from retrieved TCWV. Our error correction reduces the ζ_2 error from 53.1 % to 1.4 %. Figure 3(b) shows that errors in the sensitivity $dTCWV_{ret}/dTCWV$, which is the emulator parameter a_1 in Eq. (4), shift S_2 but do not substantially affect the gradient over r=0.5—1 km, and this conclusion also applies in Figure 3(c) when biases in a_1 are combined with σ_ε and the error correction is applied. These results show that even large biases in a_1, which contribute proportionally to estimates of errors in σ_x, do not have a substantial effect on derived scaling properties.

The final panel Figure 3(d) confirms that scaling properties are sensitive to the measurement resolution, with derived exponents varying unpredictably from 0.61—0.73 with resolution. For Δx=250 m there are only 5 points included in the regression. Furthermore, more footprints will be partially cloudy, meaning that the samples included will be too small for robust estimation of ζ_2. We did not apply a matched cloud mask for this test, and expect that this will lead to a more uncertain estimates of ζ_2. Tests across all 23 snapshots show that most return a higher, and more uncertain, ζ_2 when spatial resolution is degraded (not shown). This points to new information being obtained from finer-spatial-resolution retrievals, provided that the slanted solar paths do not destroy the correspondence between true and retrieved ζ_2.

3.3 Solar zenith angle, calculation direction and ζ_2

In our final tests we compare ζ_2 calculated on the $TCWV_{ret}$ fields with SZA changed from 15—60° as a function of the "true" value obtained from the TCWV field. The $TCWV_{ret}$ values are those using each simulation's emulator parameters and include the random error correction, while the true values refer to the columns directly over each footprint with no retrieval error. All use Δx=40—50 m with fits calculated over r=500—1000 m, and calculations are either along the y axis and parallel to the solar azimuth, or along the x axis and perpendicular to the solar azimuth.

Figure 4 shows that there is substantial spread introduced for realistic SZA, with a strong tendency for bias in ζ_2 to increase with SZA when calculated parallel to the solar azimuth. This spread and apparent bias is greatly reduced when the calculation is performed perpendicular to the solar azimuth. In the parallel case there are still significant differences (p<0.05) between true and retrieved ζ_2. The p=0.05 value threshold is calculated as 1.96 times the standard error of the difference in best-fit parameters derived from the $\ln(S_2)$ as a function of $\ln(r)$ gradient.

https://doi.org/10.5194/amt-2021-163
Preprint. Discussion started: 11 August 2021


Atmospheric Measurement Techniques Discussions

Figure 5 shows that both bias and error range expand with SZA when calculating in the solar azimuth direction, but the median (and mean, not shown) bias is eliminated by calculating S_2 in the direction perpendicular to the solar azimuth. The spread is also wider in the parallel case, the 5—95 % range of differences relative to the truth is -0.04—0.49 versus -0.20—0.22 when calculating perpendicular, while the standard deviation is 0.18 for parallel versus 0.13 for perpendicular.

These results show that realistic SZA result in path-integrated water vapour structures that have somewhat different characteristics at a 0.5—1 km scale than that of the $PCWV_{PBL}$ over each footprint. This results in additional error to estimated ζ_2, but appropriate calculation strategies that account for solar azimuth angle can reduce the magnitude of this error and suppress systematic error.

4 Discussion and conclusions

We have shown that for the q fields simulated in five LES runs of shallow convective PBLs, a novel strategy accounting for solar azimuth eliminates the SZA-induced bias in calculated ζ_2 over r of 0.5—1 km from high-spatial-resolution VSWIR retrievals. This substantially increases the range of applicable scattering geometries for which VSWIR retrievals can be used to estimate spatial scaling statistics. For example, in the airborne case studies of Thompson et al. (2021), only flight lines with SZA<15° could be used, while our method promises unbiased estimates of sub-km ζ_2 for SZA up to 60°. Removal of the bias is particularly important for applications, since q-scaling analyses using spaceborne data typically group or average over many sets of measurements (e.g. Kahn and Teixeira (2009)), and this averaging will not reduce bias in the way that it reduces RMSE. For the first time it also allows calculation of high-resolution ζ_2 statistics over midlatitude and polar areas of the globe that do not experience low solar zenith angles.

This approach should be applicable to any instrument that obtains TCWV from VSWIR with horizontal resolution approaching 50 m, not just EMIT. Operationally, this requires sufficiently long, continuous sampling perpendicular to the solar azimuth. We have not analysed length requirements here, but note that for airborne campaigns this is easily addressed on a flight-to-flight basis. For spaceborne instruments, the sampling will depend on the swath size and orbital geometry. EMIT's approximately 75 km swath (Bradley et al., 2020) spans distances larger than those considered here, and so we expect sampling to be sufficient regardless of orbital configuration. Similarly, ESA's CHIME contractor notes a 128 km swath, and similar capacities are expected for the missions that address NASA's Surface Biology and Geology (SBG) and Aerosols, Clouds, Convection and Precipitation (ACCP) designated observables. However, we note that it will be necessary to understand the implications of non-uniform footprint size and footprint-dependent errors determined from the on-orbit instrument performance in order to increase the confidence in estimates of ζ_2 from these spaceborne sensors.

Our analysis is based on the retrieval outputs of Richardson et al. (2021), which showed how random retrieval error σ_ε can be identified and removed from $TCWV_{ret}$ fields by exploiting the properties of TCWV S_2 at small scales. It also showed that errors in the T and q profiles assumed in the retrieval could affect retrieval sensitivity a_1=$dTCWV_{ret}$/dTCWV. We have shown

https://doi.org/10.5194/amt-2021-163
Preprint. Discussion started: 11 August 2021


Atmospheric Measurement Techniques Discussions

here that to obtain ζ_2 it is critical to remove the effect of σ_ε, but that while errors in a_1 are the largest error source for estimates of spatial standard deviation, they do not greatly affect the ζ_2.

Ideally this sampling strategy could be field tested, and a strategy to do so would be to perform flights both parallel and perpendicular to the solar azimuth with collocated retrievals of TCWV from VSWIR and an independent instrument that is not affected by SZA, such as a differential absorption lidar (DIAL) or passive sounding instrument. The non-VSWIR instrument would allow calculation of ζ_2 that is not affected by sunlight path, and the conclusions of this study would be supported if the VSWIR and non-VSWIR estimates showed good agreement for the perpendicular but not parallel flight paths. We highlight the High Altitude Lidar Observatory (Bedka et al., 2021) as a candidate sensor for such an experiment.

For science applications, it would also be necessary to identify which scenes are likely to satisfy our requirements, for example conditions proximate to deep convection may have more substantial above-PBL variability at <1 km scales and result in weaker correspondence between TCWV and $PCWV_{PBL}$. In addition, it may be necessary to identify PBL height, which would require independent information from weather forecast models or reanalysis, *in situ* measurements or other instruments. Furthermore, users would also need to consider the effect of sampling biases that may depend on cloud fraction or on the presence of non-isotropic variability in features such as horizontal convective rolls (e.g. as explored in Carbajal Henken et al. (2015)). If locations commonly experience meteorological features with a preferential orientation, for example due to orography or a coastline, then this method may not adequately capture its full structure.

Finally, the interpretation of these exponents has not been considered in detail here but future work could proceed either observationally or theoretically. For an observational study, the relationship between retrieved exponents and other properties, such as later convective initiation could be investigated. A theoretical study would need to apply current understanding of turbulent physics to address precisely the problem of the horizontal variability of vertically-averaged profiles. Further in the future, perhaps multi-angle imaging spectroscopy could provide profiling from VSWIR measurements via computed tomography, which has been demonstrated to retrieve aerosol profiles in some conditions using the Multi-Angle Imaging SpectroRadiometer (MISR) on Terra (Garay et al., 2016) and upper-tropospheric water vapour profiles from airborne measurements with the Gimballed Limb Observer for Radiance Imaging of the Atmosphere (GLORIA, Ungermann et al. (2015)). We are not aware of any likely short-term space missions that would allow water vapour tomography from VSWIR retrievals at EMIT-like horizontal resolution, with the upcoming Multiangle Imager for Aerosols (MAIA, Diner et al. (2018)) having horizontal resolution similar to that of MODIS. If such an instrument were launched, high-spatial-resolution tomography would also be subject to the smearing effect from the non-vertical solar path and so may benefit from our proposal, although a detailed study of the particular instrument and retrieval setup would be required.

Our main conclusion is that a novel sampling strategy can allow a breakthrough in space-based measurement of PBL water vapour scaling, and that while individual uncertainties and geographical sampling may vary with the mission, this principle will apply to the array of upcoming VSWIR instruments whose spectra will allow column water vapour retrievals at resolutions from 30—80 m or better. The resulting statistics offer a new check on the validity of high-resolution atmospheric models and inform sub-grid parameterisations of coarser ESMs.

https://doi.org/10.5194/amt-2021-163
Preprint. Discussion started: 11 August 2021

Atmospheric Measurement Techniques Discussions

Acknowledgments: This research was carried out at the Jet Propulsion Laboratory, California Institute of Technology, Pasadena, CA, USA, under contract with the National Aeronautics and Space Administration. MR thanks Amin Nehrir and Brian Carroll of NASA Langley for helpful discussion regarding HALO lidar data.

References

Arakawa, A., Jung, J.-H. and Wu, C.-M.: Toward unification of the multiscale modeling of the atmosphere, Atmos. Chem. Phys., 11(8), 3731–3742, doi:10.5194/acp-11-3731-2011, 2011.

Bacmeister, J. T., Eckermann, S. D., Newman, P. A., Lait, L., Chan, K. R., Loewenstein, M., Proffitt, M. H. and Gary, B. L.: Stratospheric horizontal wavenumber spectra of winds, potential temperature, and atmospheric tracers observed by high-altitude aircraft, J. Geophys. Res. Atmos., 101(D5), 9441–9470, doi:10.1029/95JD03835, 1996.

Bedka, K. M., Nehrir, A. R., Kavaya, M., Barton-Grimley, R., Beaubien, M., Carroll, B., Collins, J., Cooney, J., Emmitt, G. D., Greco, S., Kooi, S., Lee, T., Liu, Z., Rodier, S. and Skofronick-Jackson, G.: Airborne Lidar Observations of Wind, Water Vapor, and Aerosol Profiles During The NASA Aeolus Cal/Val Test Flight Campaign, Atmos. Meas. Tech. Discuss., doi:10.5194/amt-2020-475, 2021.

Berk, A., Conforti, P., Kennett, R., Perkins, T., Hawes, F. and van den Bosch, J.: MODTRAN6: a major upgrade of the MODTRAN radiative transfer code, in Proceedings Volume 9088, Algorithms and Technologies for Multispectral, Hyperspectral, and Ultraspectral Imagery XX, edited by M. Velez-Reyes and F. A. Kruse, p. 90880H, Baltimore, MD, USA., 2014.

Berk, A., Conforti, P. and Hawes, F.: An accelerated line-by-line option for MODTRAN combining on-the-fly generation of line center absorption within 0.1 cm-1 bins and pre-computed line tails, in Proceedings Volume 9472, Algorithms and Technologies for Multispectral, Hyperspectral, and Ultraspectral Imagery XXI, edited by M. Velez-Reyes and F. A. Kruse, p. 947217, Baltimore, MD, USA., 2015.

Boffetta, G., De Lillo, F., Mazzino, A. and Musacchio, S.: Bolgiano scale in confined Rayleigh–Taylor turbulence, J. Fluid Mech., 690, 426–440, doi:10.1017/jfm.2011.446, 2012.

Bolgiano, R.: Turbulent spectra in a stably stratified atmosphere, J. Geophys. Res., 64(12), 2226–2229, doi:10.1029/JZ064i012p02226, 1959.

Bradley, C. L., Thingvold, E., Moore, L. B., Haag, J. M., Raouf, N. A., Mouroulis, P. and Green, R. O.: Optical design of the Earth Surface Mineral Dust Source Investigation (EMIT) imaging spectrometer, in Imaging Spectrometry XXIV: Applications, Sensors, and Processing, edited by P. Mouroulis and E. J. Ientilucci, p. 1, SPIE., 2020.

Brown, A. R., Cederwall, R. T., Chlond, A., Duynkerke, P. G., Golaz, J.-C., Khairoutdinov, M., Lewellen, D. C., Lock, A. P., MacVean, M. K., Moeng, C.-H., Neggers, R. A. J., Siebesma, A. P. and Stevens, B.: Large-eddy simulation of the diurnal cycle of shallow cumulus convection over land, Q. J. R. Meteorol. Soc., 128(582), 1075–1093, doi:10.1256/003590002320373210, 2002.

https://doi.org/10.5194/amt-2021-163
Preprint. Discussion started: 11 August 2021


Atmospheric Measurement Techniques Discussions

Candela, L., Formaro, R., Guarini, R., Loizzo, R., Longo, F. and Varacalli, G.: The PRISMA mission, in 2016 IEEE International Geoscience and Remote Sensing Symposium (IGARSS), pp. 253–256, IEEE., 2016.

Carbajal Henken, C. K., Diedrich, H., Preusker, R. and Fischer, J.: MERIS full-resolution total column water vapor: Observing horizontal convective rolls, Geophys. Res. Lett., 42(22), 10,074-10,081, doi:10.1002/2015GL066650, 2015.

Cho, J. Y. N., Zhu, Y., Newell, R. E., Anderson, B. E., Barrick, J. D., Gregory, G. L., Sachse, G. W., Carroll, M. A. and Albercook, G. M.: Horizontal wavenumber spectra of winds, temperature, and trace gases during the Pacific Exploratory Missions: 1. Climatology, J. Geophys. Res. Atmos., 104(D5), 5697–5716, doi:10.1029/98JD01825, 1999.

Diner, D. J., Boland, S. W., Brauer, M., Bruegge, C., Burke, K. A., Chipman, R., Di Girolamo, L., Garay, M. J., Hasheminassab, S. and Hyer, E.: Advances in multiangle satellite remote sensing of speciated airborne particulate matter and association with adverse health effects: from MISR to MAIA, J. Appl. Remote Sens., 12(04), 1, doi:10.1117/1.JRS.12.042603, 2018.

Dorrestijn, J., Kahn, B. H., Teixeira, J. and Irion, F. W.: Instantaneous variance scaling of AIRS thermodynamic profiles using a circular area Monte Carlo approach, Atmos. Meas. Tech., 11(5), 2717–2733, doi:10.5194/amt-11-2717-2018, 2018.

Drusch, M., Del Bello, U., Carlier, S., Colin, O., Fernandez, V., Gascon, F., Hoersch, B., Isola, C., Laberinti, P., Martimort, P., Meygret, A., Spoto, F., Sy, O., Marchese, F. and Bargellini, P.: Sentinel-2: ESA's Optical High-Resolution Mission for GMES Operational Services, Remote Sens. Environ., 120, 25–36, doi:10.1016/j.rse.2011.11.026, 2012.

Fischer, L., Kiemle, C. and Craig, G. C.: Height-resolved variability of midlatitude tropospheric water vapor measured by an airborne lidar, Geophys. Res. Lett., 39(6), n/a-n/a, doi:10.1029/2011GL050621, 2012.

Fischer, L., Craig, G. C. and Kiemle, C.: Horizontal structure function and vertical correlation analysis of mesoscale water vapor variability observed by airborne lidar, J. Geophys. Res. Atmos., 118(14), 7579–7590, doi:10.1002/jgrd.50588, 2013.

Gage, K. S. and Nastrom, G. D.: On the spectrum of atmospheric velocity fluctuations seen by MST/ST radar and their interpretation, Radio Sci., 20(6), 1339–1347, doi:10.1029/RS020i006p01339, 1985.

Garay, M. J., Davis, A. B. and Diner, D. J.: Tomographic reconstruction of an aerosol plume using passive multiangle observations from the MISR satellite instrument, Geophys. Res. Lett., 43(24), doi:10.1002/2016GL071479, 2016.

Gelaro, R., McCarty, W., Suárez, M. J., Todling, R., Molod, A., Takacs, L., Randles, C. A., Darmenov, A., Bosilovich, M. G., Reichle, R., Wargan, K., Coy, L., Cullather, R., Draper, C., Akella, S., Buchard, V., Conaty, A., da Silva, A. M., Gu, W., Kim, G.-K., Koster, R., Lucchesi, R., Merkova, D., Nielsen, J. E., Partyka, G., Pawson, S., Putman, W., Rienecker, M., Schubert, S. D., Sienkiewicz, M. and Zhao, B.: The Modern-Era Retrospective Analysis for Research and Applications, Version 2 (MERRA-2), J. Clim., 30(14), 5419–5454, doi:10.1175/JCLI-D-16-0758.1, 2017.

Golaz, J.-C., Larson, V. E. and Cotton, W. R.: A PDF-Based Model for Boundary Layer Clouds. Part I: Method and Model Description, J. Atmos. Sci., 59(24), 3540–3551, doi:10.1175/1520-0469(2002)059<3540:APBMFB>2.0.CO;2, 2002.

Green, R. O. and Thompson, D. R.: An Earth Science Imaging Spectroscopy Mission: The Earth Surface Mineral Dust Source Investigation (EMIT), in IGARSS 2020 - 2020 IEEE International Geoscience and Remote Sensing Symposium, pp. 6262–6265, IEEE., 2020.

Kahn, B. H. and Teixeira, J.: A Global Climatology of Temperature and Water Vapor Variance Scaling from the Atmospheric Infrared Sounder, J. Clim., 22(20), 5558–5576, doi:10.1175/2009JCLI2934.1, 2009.

Kahn, B. H., Teixeira, J., Fetzer, E. J., Gettelman, A., Hristova-Veleva, S. M., Huang, X., Kochanski, A. K., Köhler, M., Krueger, S. K., Wood, R. and Zhao, M.: Temperature and Water Vapor Variance Scaling in Global Models: Comparisons to Satellite and Aircraft Data, J. Atmos. Sci., 68(9), 2156–2168, doi:10.1175/2011JAS3737.1, 2011.

Krutz, D., Müller, R., Knodt, U., Günther, B., Walter, I., Sebastian, I., Säuberlich, T., Reulke, R., Carmona, E., Eckardt, A., Venus, H., Fischer, C., Zender, B., Arloth, S., Lieder, M., Neidhardt, M., Grote, U., Schrandt, F., Gelmi, S. and Wojtkowiak, A.: The Instrument Design of the DLR Earth Sensing Imaging Spectrometer (DESIS), Sensors, 19(7), 1622, doi:10.3390/s19071622, 2019.

Kunnen, R. P. J., Clercx, H. J. H., Geurts, B. J., van Bokhoven, L. J. A., Akkermans, R. A. D. and Verzicco, R.: Numerical and experimental investigation of structure-function scaling in turbulent Rayleigh-Bénard convection, Phys. Rev. E, 77(1), 016302, doi:10.1103/PhysRevE.77.016302, 2008.

Kurowski, M. J., Grabowski, W. W. and Smolarkiewicz, P. K.: Anelastic and Compressible Simulation of Moist Dynamics at Planetary Scales, J. Atmos. Sci., 72(10), 3975–3995, doi:10.1175/JAS-D-15-0107.1, 2015.

Kurowski, M. J., Grabowski, W. W., Suselj, K. and Teixeira, J.: The Strong Impact of Weak Horizontal Convergence on Continental Shallow Convection, J. Atmos. Sci., 77(9), 3119–3137, doi:10.1175/JAS-D-19-0351.1, 2020.

Lovejoy, S., Schertzer, D. and Tuck, A. F.: Fractal aircraft trajectories and nonclassical turbulent exponents, Phys. Rev. E, 70(3), 036306, doi:10.1103/PhysRevE.70.036306, 2004.

Lovejoy, S., Tuck, A. F., Hovde, S. J. and Schertzer, D.: Is isotropic turbulence relevant in the atmosphere?, Geophys. Res. Lett., 34(15), doi:10.1029/2007GL029359, 2007.

Matheou, G. and Chung, D.: Large-Eddy Simulation of Stratified Turbulence. Part II: Application of the Stretched-Vortex Model to the Atmospheric Boundary Layer, J. Atmos. Sci., 71(12), 4439–4460, doi:10.1175/JAS-D-13-0306.1, 2014.

Obukhov, A. M.: On the influence of buoyancy forces on the structure of the temperature field in a turbulent flow, Dokl. Acad. Nauk. SSST., 125, 1959.

Perraud, E., Couvreux, F., Malardel, S., Lac, C., Masson, V. and Thouron, O.: Evaluation of Statistical Distributions for the Parametrization of Subgrid Boundary-Layer Clouds, Boundary-Layer Meteorol., 140(2), 263–294, doi:10.1007/s10546-011-9607-3, 2011.

Pinel, J., Lovejoy, S., Schertzer, D. and Tuck, A. F.: Joint horizontal-vertical anisotropic scaling, isobaric and isoheight wind statistics from aircraft data, Geophys. Res. Lett., 39(11), n/a-n/a, doi:10.1029/2012GL051689, 2012.

Pressel, K. G. and Collins, W. D.: First-Order Structure Function Analysis of Statistical Scale Invariance in the AIRS-Observed Water Vapor Field, J. Clim., 25(16), 5538–5555, doi:10.1175/JCLI-D-11-00374.1, 2012.

Prusa, J. M., Smolarkiewicz, P. K. and Wyszogrodzki, A. A.: EULAG, a computational model for multiscale flows, Comput. Fluids, 37(9), 1193–1207, doi:10.1016/j.compfluid.2007.12.001, 2008.

Rast, M., Ananasso, C., Bach, H., Ben-Dor, E., Chabrillat, S., Colombo, R., Del Bello, U., Feret, J., Giardino, C., Green, R.,

Guanter, L., Marsh, S., Nieke, J., CCH, O., Rum, G., Schaepman, M., Schlerf, M., Skidmore, A. and Strobl, P.: Copernicus hyperspectral imaging mission for the environment: Mission requirements document version 2.1, Frascati, Italy., 2019.

Richardson, M., Thompson, D. R., Kurowski, M. J. and Lebsock, M. D.: Boundary layer water vapour statistics from high spatial resolution spaceborne visible spectrometry, Atmos. Meas. Tech. Discuss., 2021.

Schemann, V., Stevens, B., Grützun, V. and Quaas, J.: Scale Dependency of Total Water Variance and Its Implication for Cloud Parameterizations, J. Atmos. Sci., 70(11), 3615–3630, doi:10.1175/JAS-D-13-09.1, 2013.

Selz, T., Fischer, L. and Craig, G. C.: Structure Function Analysis of Water Vapor Simulated with a Convection-Permitting Model and Comparison to Airborne Lidar Observations, J. Atmos. Sci., 74(4), 1201–1210, doi:10.1175/JAS-D-16-0160.1, 2017.

Siebesma, A. P., Bretherton, C. S., Brown, A., Chlond, A., Cuxart, J., Duynkerke, P. G., Jiang, H., Khairoutdinov, M., Lewellen, D., Moeng, C.-H., Sanchez, E., Stevens, B. and Stevens, D. E.: A Large Eddy Simulation Intercomparison Study of Shallow Cumulus Convection, J. Atmos. Sci., 60(10), 1201–1219, doi:10.1175/1520-0469(2003)60<1201:ALESIS>2.0.CO;2, 2003.

Skamarock, W. C., Park, S.-H., Klemp, J. B. and Snyder, C.: Atmospheric Kinetic Energy Spectra from Global High-Resolution Nonhydrostatic Simulations, J. Atmos. Sci., 71(11), 4369–4381, doi:10.1175/JAS-D-14-0114.1, 2014.

Sommeria, G. and Deardorff, J. W.: Subgrid-Scale Condensation in Models of Nonprecipitating Clouds, J. Atmos. Sci., 34(2), 344–355, doi:10.1175/1520-0469(1977)034<0344:SSCIMO>2.0.CO;2, 1977.

Szczodrak, M., Austin, P. H. and Krummel, P. B.: Variability of Optical Depth and Effective Radius in Marine Stratocumulus Clouds, J. Atmos. Sci., 58(19), 2912–2926, doi:10.1175/1520-0469(2001)058<2912:VOODAE>2.0.CO;2, 2001.

Thompson, D. R., Natraj, V., Green, R. O., Helmlinger, M. C., Gao, B.-C. and Eastwood, M. L.: Optimal estimation for imaging spectrometer atmospheric correction, Remote Sens. Environ., 216, 355–373, doi:10.1016/j.rse.2018.07.003, 2018.

Thompson, D. R., Cawse-Nicholson, K., Erickson, Z., Fichot, C. G., Frankenberg, C., Gao, B.-C., Gierach, M. M., Green, R. O., Jensen, D., Natraj, V. and Thompson, A.: A unified approach to estimate land and water reflectances with uncertainties for coastal imaging spectroscopy, Remote Sens. Environ., 231, 111198, doi:10.1016/j.rse.2019.05.017, 2019.

Thompson, D. R., Kahn, B. H., Brodrick, P. G., Lebsock, M. D., Richardson, M. and Green, R. O.: Spectroscopic imaging of sub-kilometer spatial structure in lower-tropospheric water vapor, Atmos. Meas. Tech., 14(4), 2827–2840, doi:10.5194/amt-14-2827-2021, 2021.

Ungermann, J., Blank, J., Dick, M., Ebersoldt, A., Friedl-Vallon, F., Giez, A., Guggenmoser, T., Höpfner, M., Jurkat, T., Kaufmann, M., Kaufmann, S., Kleinert, A., Krämer, M., Latzko, T., Oelhaf, H., Olchewski, F., Preusse, P., Rolf, C., Schillings, J., Suminska-Ebersoldt, O., Tan, V., Thomas, N., Voigt, C., Zahn, A., Zöger, M. and Riese, M.: Level 2 processing for the imaging Fourier transform spectrometer GLORIA: derivation and validation of temperature and trace gas volume mixing ratios from calibrated dynamics mode spectra, Atmos. Meas. Tech., 8(6), 2473–2489, doi:10.5194/amt-8-2473-2015, 2015.

vanZanten, M. C., Stevens, B., Nuijens, L., Siebesma, A. P., Ackerman, A. S., Burnet, F., Cheng, A., Couvreux, F., Jiang, H., Khairoutdinov, M., Kogan, Y., Lewellen, D. C., Mechem, D., Nakamura, K., Noda, A., Shipway, B. J., Slawinska, J., Wang,

https://doi.org/10.5194/amt-2021-163
Preprint. Discussion started: 11 August 2021

Atmospheric Measurement Techniques Discussions

S. and Wyszogrodzki, A.: Controls on precipitation and cloudiness in simulations of trade-wind cumulus as observed during RICO, J. Adv. Model. Earth Syst., 3(2), M06001, doi:10.1029/2011MS000056, 2011.

Wroblewski, D. E., Coté, O. R., Hacker, J. M. and Dobosy, R. J.: Velocity and Temperature Structure Functions in the Upper Troposphere and Lower Stratosphere from High-Resolution Aircraft Measurements, J. Atmos. Sci., 67(4), 1157–1170, doi:10.1175/2009JAS3108.1, 2010.

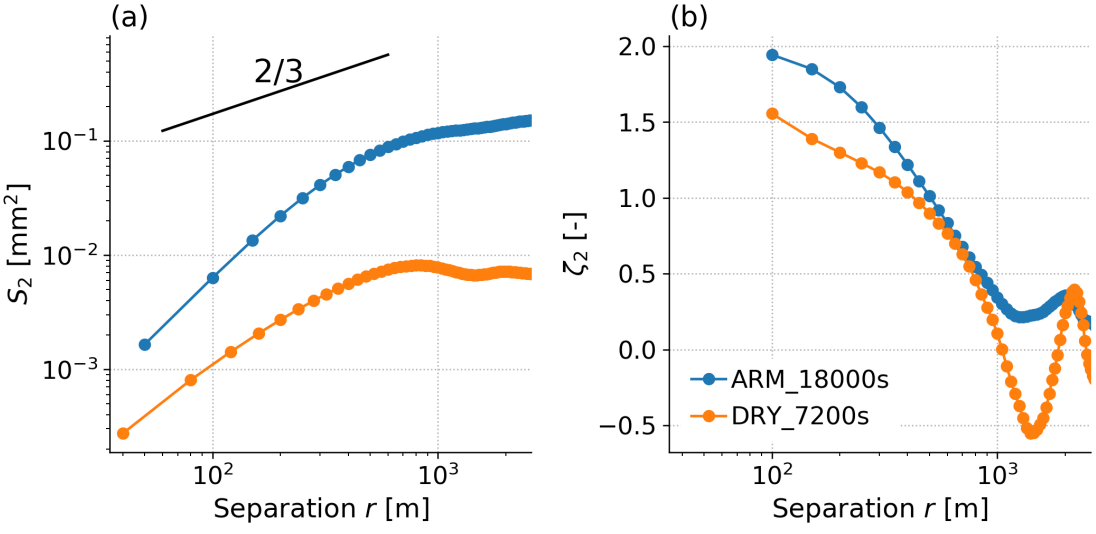

Figure 1. (a) S_2 calculated from TCWV for two LES snapshots as a function of separation distance, with the 2/3 gradient associated with a passive tracer in turbulence following Kolmogorov theory also shown, (b) exponent calculated locally at each separation distance

https://doi.org/10.5194/amt-2021-163
Preprint. Discussion started: 11 August 2021

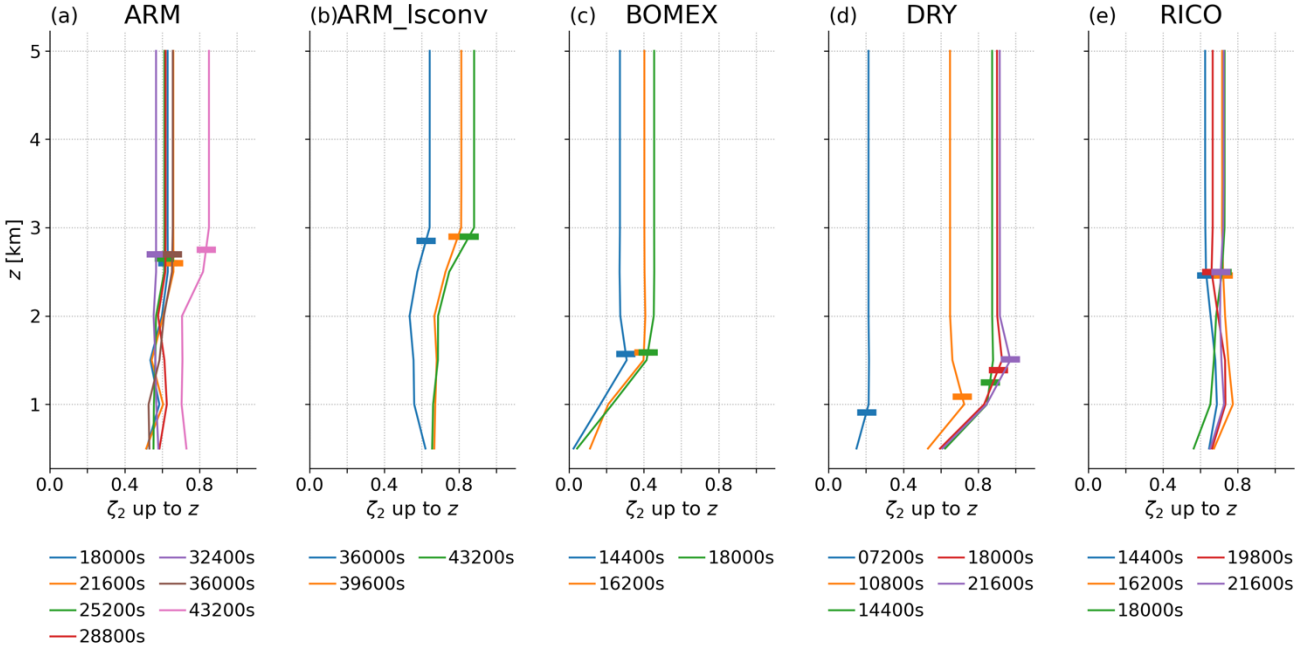

Figure 2. Calculated structure function exponents using separation distance 0.5—1 km directly on LES output, calculated for integrated water vapour up to each labelled capping altitude, every 0.5 km. The PBL top derived from the location of the maximum vertical gradient in potential temperature is shown as a horizontal bar for each profile.

https://doi.org/10.5194/amt-2021-163
Preprint. Discussion started: 11 August 2021

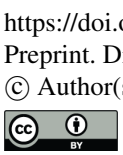

Atmospheric Measurement Techniques Discussions

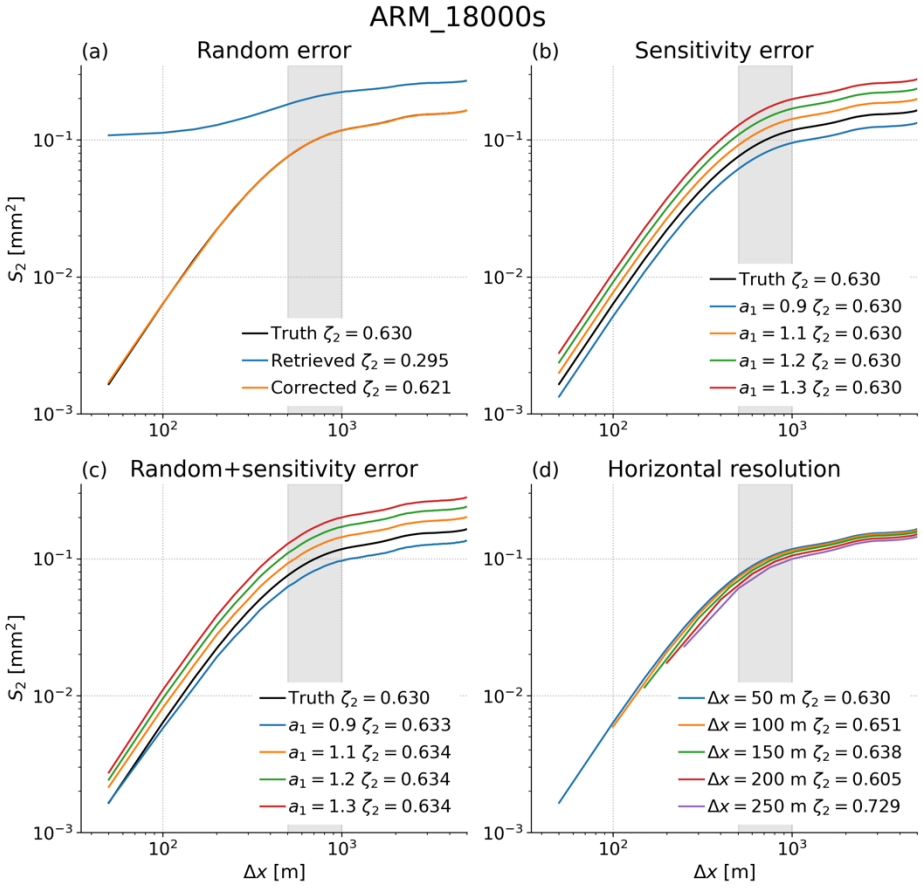

Figure 3. Sensitivity of derived S_2 to retrieval errors and spatial resolution, the legends in each case report the calculated exponent from a fit over separations 0.5—1 km, the region which is shaded grey in each panel. In each case "truth" refers to the value calculated from TCWV at native LES resolution of 50 m. (a) blue shows S_2 derived from retrieved TCWV including random error only, and orange the S_2 after subtracting the estimated retrieval variance. (b) S_2 calculated with no random error, but non-unity sensitivity $dTCWV_{ret}/dTCWV$ as defined by the a_1 trend parameter in Eq. (4). (c) The result when combining random error and sensitivity error, after subtraction of the random error estimated from each retrieved field. (d) S_2 calculated after smoothing the field resolution sequentially to 250 m × 250 m.

https://doi.org/10.5194/amt-2021-163
Preprint. Discussion started: 11 August 2021

Atmospheric Measurement Techniques Discussions

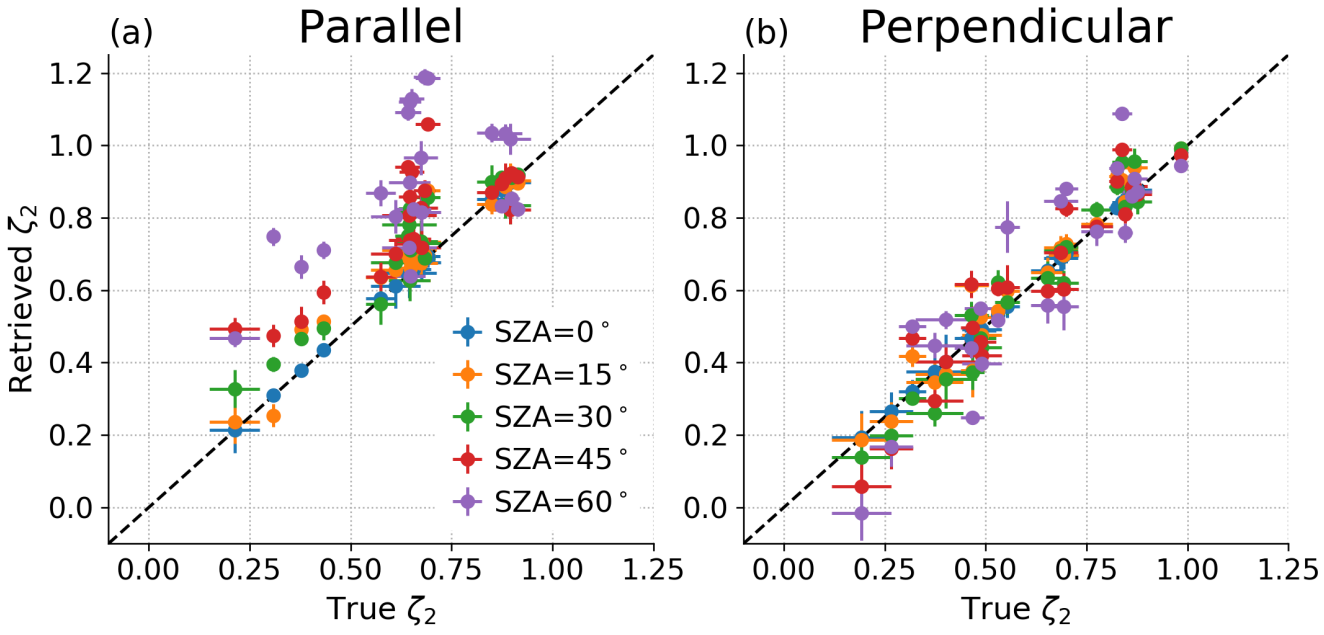

Figure 4. Estimated clear-sky ζ_2 over separations 0.5—1 km in all 23 snapshots as a function of the true value. The error bars are ±2σ from the trend fit.

5

https://doi.org/10.5194/amt-2021-163
Preprint. Discussion started: 11 August 2021

Atmospheric Measurement Techniques Discussions

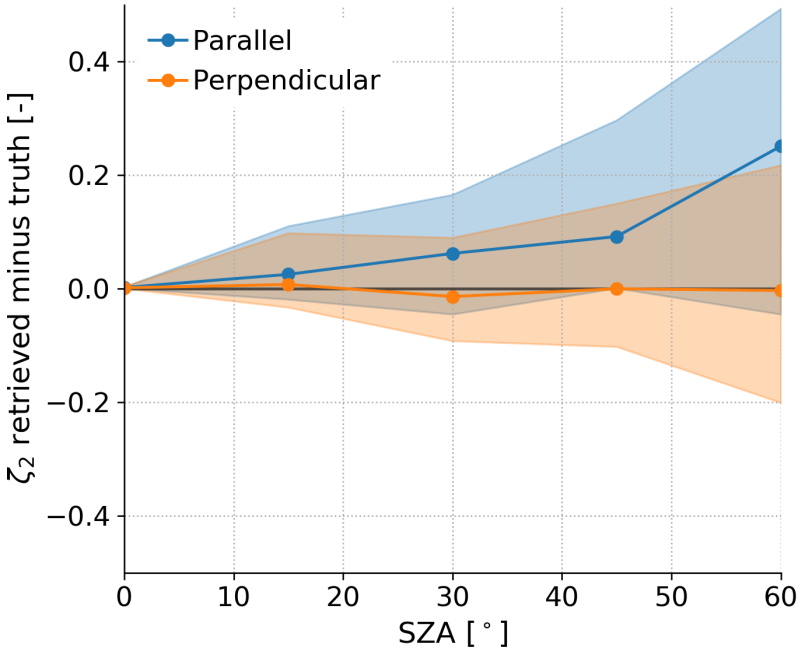

Figure 5. Median and 5—95 % range of retrieved minus true ζ_2 as a function of solar zenith angle. "Parallel" refers to calculation along the solar azimuth direction, and "Perpendicular" refers to calculation perpendicular to it.